POLITECNICO DI TORINO

Master's Degree in Communication and Computer Networks Engineering

Master's Degree Thesis

Inverse source methods: near-field to near-field and far-field reconstruction

Supervisors

Prof. Giuseppe VECCHI

Dr. Marco RIGHERO

Dr. Giorgio GIORDANENGO

Candidate

DUO JING

September 2022

Summary

This thesis describes different formulations based on the inverse source problem, the equivalent source or field is calculated on an arbitrary 3D closed surface based on complex vector electric field data on a specified (external) surface. According to the equivalence principle analysis formula, the possible choices of internal fields are analyzed, as well as their practical effects. The Love equivalence that the zero interior field yields electric and magnetic currents related to the of the electric and magnetic fields on the reconstruction surface. A single current (electric or magnetic) formula derived from the continuity of a single field is used in the different constrains forced. The single equation formulation is simpler to implement and has a lower computational load than the dual-equation formulation, but the latter will perform better in numerical tests of synthetic data.In this paper, three inverse source methods are adopted to reconstruct the same electric field data, and the stability and effectiveness of the inverse source methods in various reconstruction surfaces are verified by testing the accuracy of the three inverse source methods in different fields and comparing their performance.

Acknowledgements

I have received a lot of help and gained a lot from people during this long thesis project

I would like to thank my advisor, prof. Giuseppe Vecchi for guiding and supporting me over the years. You have set an example of excellence as a researcher, mentor, instructor, and role model.

I would like to thank my supervisor Dr. Marco Righero for all of his guidance through this process; your discussion, ideas, and feedback have been absolutely invaluable.

I'd like to thank my fellow graduate students, research technicians, collaborators, and the multitude of undergraduates who contributed to this research. I am very grateful to all of you.

In addition, I would like to thank my parents for their wise counsel and sympathetic ear. You are always there for me.

Jing Duo

Table of Contents

List of Tables

List of Figures

Chapter 1

Introduction

As antenna engineering develops, inverse source reconstruction techniques have various applications such as field measurements, compact antenna representations and near-field to far-field (NF-FF) transformations.The source reconstruction problem is a linear inverse problem, where the current at a known location is obtained from a given complex radiation vector field (known from measurements), and then the information about the field at a location is calculated from the current.This problem can be formulated in terms of some integral equations, the computational problems of which have been solved by these articles. In [1], the near-field to far-field transformation under equivalent currents in the infinite extension plane is explained, concerning probability of global equivalence. In [2], the global field extrapolation problem is solved from its knowledge in a finite region using the equivalent magnetic current located in the infinite PEC (perfect electrical conductor) plane. In [3], the author did the dual (electric currents/Perfect Magnetic Conductor (PMC)).In [4], it was shown that the far field is computed in near-field measurements over a limited range. In [5], equivalent magnetic currents are reported for small antenna diagnostics; In [6], source reconstruction techniques were used to characterize commercial antennas from measurements in a limited canonical range using a model based on equivalent magnetic currents in the plane. In [7], a novel diagnostic application is presented of the source reconstruction technique, whereby disturbances present in measurements due to unwanted interaction with neighboring objects are removed in a post processing step. In [8] introduced the dual-equation formulation for the general vector problem on 3-D surfaces and showed its advantages over the widespread single-equation formulation.

This paper will be devoted to investigate the electric field reconstruction performance of three inverse source methods for three different antenna models. The advantages and disadvantages of the three inverse source methods are compared and the focus is on the transforms from near-field to near-field and from near-field to far-field.The section on near-field studies will also focus on the analysis of the electric field reconstruction inside the equivalent current surface and the electric field reconstruction outside.

The main structure of this paper is as follows. In Chapter 2, the principles and formulas of the three inverse source methods are introduced. In chapter 3 presents the antenna model used. In chapter 4 the inverse source methods are discussed in the near-field to near-field and in chapter 5 the near-field to far-field transforms are discussed. And make some conclusion in chapter 6.

Chapter 2

Inverse equivalent surface-source solution

Consider an inverse equivalent surface-source formulation as portrayed in Fig 2.1. The input data for this problem are the values of the electric field tangent to a specified measurement surface denoted by Σ_M, generally speaking Σ_M is a surface further away from the antenna structure than the reconstruction surface Σ_R. Typically, Σ_M is a closed sphere or cylinder surface, and may be open (like a finite cylinder, or a finite planar domain). The aim is to find the source on a closed reconstruction surface, denoted by Σ_R, to radiate the input electrical field on Σ_M. In some cases one may also be interested in the actual field values on Σ_R, not just current source.

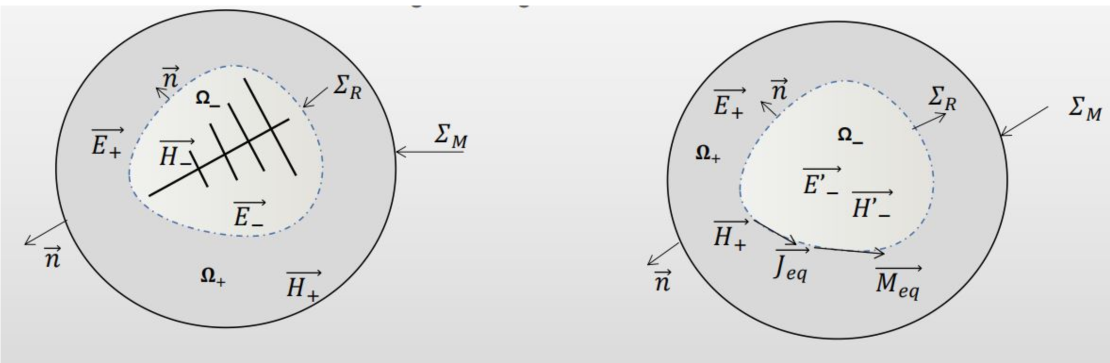

Figure 2.1: Illustration of the Equivalence Principle: Original (left) and general equivalent problem (right)

Taking into account the original radiation problem, depicted in Fig 2.1 (left): the volume Ω_- contains all the original sources, and all material bodies (like antenna conductors, other obstacles, etc.), while the external region is in free space. In the external equivalent problem shown in Fig 2.1 (right), the original source and material bodies are removed and the equivalent electromagnetic currents J_{eq} and M_{eq} are placed on a closed surface called reconstruction surface Σ_R. The equivalent currents radiate identical external fields E_+, H_+, yet the original inner fields E_-, H_- are substituted by other fields, denoted by $E_-^{'}$, $H_-^{'}$. In order to achieve the field equivalence in Ω_+, these equivalent currents must obey the formulas:

$$\begin{cases} \hat{n} \times [H_+(r) - H_-^{'}(r)] = J_{eq} \\ -\hat{n} \times [E_+(r) - E_-^{'}(r)] = M_{eq} \end{cases} \quad r \in \Sigma_R \tag{2.1}$$

Where $\hat{n}$ is the unit normal vector of surface Σ_R.

Regardless of the internal field$E_-^{'}$, $H_-^{'}$, the equivalent currents J_{eq}, M_{eq} radiate in unbounded homogeneous space. Due to the removal of all internal material bodies, the field can be calculated anywhere by using the conventional free-space radiation operator:

$$E(r) = -\eta_0 \mathcal{L}(J_{eq}; r) + \mathcal{K}(M_{eq}; r) \tag{2.2}$$

where

$$\mathcal{L}(J_{eq}; r) = jk_0 \int_{\Sigma_R} [J_{eq} + \frac{1}{k_0^2} \bigtriangledown \bigtriangledown_s^{'}] \times g(r, r^{'}) ds^{'} \tag{2.3}$$

$$\mathcal{K}(M_{eq}; r) = \int_{\Sigma_R} M_{eq}(r^{'}) \times \bigtriangledown g(r, r^{'}) ds^{'} \tag{2.4}$$

$$g(r, r^{'}) = \frac{e^{-jk_0|r-r^{'}|}}{4\pi|r - r^{'}|} \tag{2.5}$$

And $\eta_0 = \sqrt{\mu_0/\epsilon_0}, k_0 = \omega\sqrt{\mu_0\epsilon_0}$, $\bigtriangledown_s^{'}$ is the surface divergence operator($r \notin \Sigma_R$).

In the following, the interior fields are set to zero and the result is Love's form of the Equivalence Principle:

$$\begin{cases} \hat{n} \times H_+(r) = J_{eq}^{Love} \\ -\hat{n} \times E_+(r) = M_{eq}^{Love} \end{cases} \quad r \in \Sigma_R \tag{2.6}$$

In the simplest case, the operator mapping the equivalent electric and magnetic current density J_{eq}^F and M_{eq}^F on the reconstruction surface Σ_R to field samples on measurement surface at a certain distance. This case is called *fitting* condition which satisfied the equation below:

$$E(J_{eq}^F) + E(M_{eq}^F) = E(r) \quad r \in \Sigma_M \tag{2.7}$$

where $E(J_{eq})$ is short notation for $E(r)$ due to J_{eq}, similarly $E(M_{eq})$ is short notation for $E(r)$ due to M_{eq} according to equation 2.2.

The second kind of operator is made of two parts: one part is the operator mapping a surface current to field samples on a measurement surface at a particular distance from the reconstruction surface, same as $fitting$ case. The adding part is Love constraint. The operator mapping the equivalent current on the reconstruction surface Σ_R should be forced to 0. This case is named *loveasside* or *loveside*. The equivalent electromagnetic surface current densities are defined as J_{eq}^S and M_{eq}^S.

$$\begin{cases} E(J_{eq}^S) + E(M_{eq}^S) = E(r) \\ E(J_{eq}^S) + E(M_{eq}^S) = E(r^{'}) = 0 \end{cases} \qquad r \in \Sigma_M, r^{'} \in \Sigma_R \tag{2.8}$$

The third possibility also be examined: firstly the equivalent electromagnetic surface current densities on the reconstruction surface Σ_R are forced matching the field samples in $fitting$ case, then the field radiates on the reconstruction surface by these electromagnetic surface currents and at last step the *Love* currents were evaluated from field samples. This case is called *lovepost*.The equivalent electromagnetic surface current densities are defined as J_{eq}^P and M_{eq}^P in this condition and they satisfy the following equations:

$$\begin{cases} E(J_{eq}^F) + E(M_{eq}^F) = E(r) \\ J_{eq}^P = \hat{n} \times (H(J_{eq}^F) + H(M_{eq}^F)) \\ M_{eq}^P = -\hat{n} \times (E(J_{eq}^F) + E(M_{eq}^F)) \end{cases} \qquad r \in \Sigma_M, r^{'} \in \Sigma_R \tag{2.9}$$

where $\hat{n}$ is the outward normal to Σ_R.

Chapter 3

Antenna structure under test

In this paper, three different antennas are simulated in CST Studio Suite at center frequency 3 GHz to collect data: dipole antenna, dipole antenna array, and patch antenna. The dipole antenna and the dipole array antenna use the same parameters, while the dipole array is just 2 single replicas of the dipole with the distance between two dipoles being half of the wavelength.

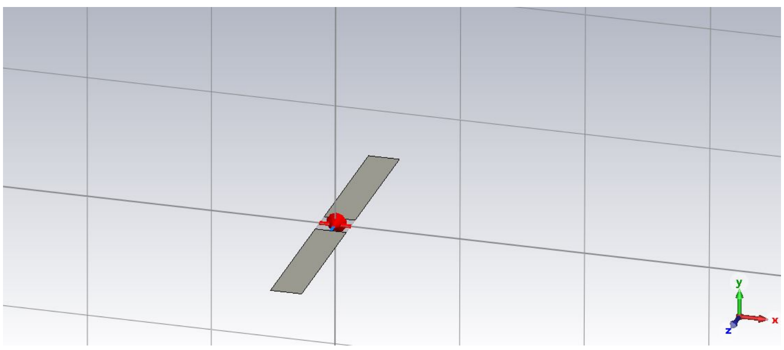

Figure 3.1: Dipole antenna along Z-direction

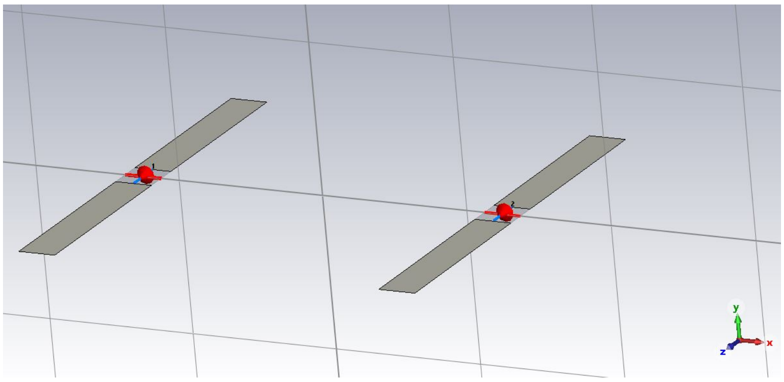

Figure 3.2: Dipole array antenna along the Z-direction

The center of both antennas is the origin of the coordinate so that the data can be rendered more intuitive and graphically symmetrical, regardless of the choice of reference coordinate system, without affecting the results. The material of antenna body is PEC (perfect electrical conductor), and the simulation of the antenna is based on vacuum environment, which will not be discussed later.

Wavelength[m]	width[m]	length[m]	gap[m]
9.99E-2	4.99E-3	4.99E-2	4.99E-3

Table 3.1: Dipole antenna parameter

The patch antenna design is more complex, but the whole can be divided into three layers: the lowermost PEC ground, the middle dielectric layer and the uppermost PEC patch.

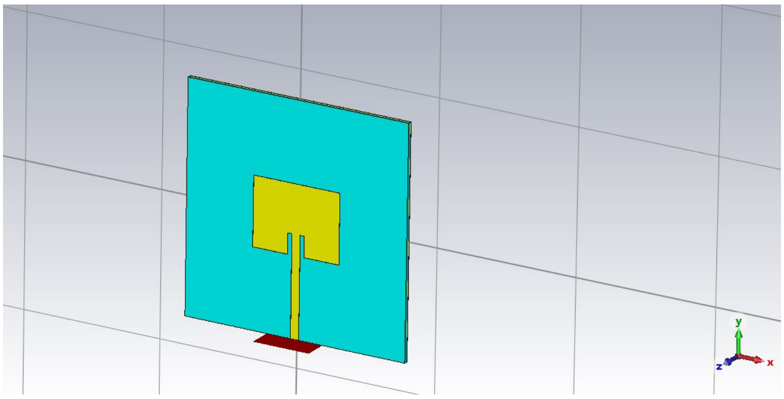

Figure 3.3: Patch antenna on XY plane

Similar to the previous dipole antenna, the center of the patch antenna is also the origin of the coordinates, but it should be noted that the patch antenna is parallel to the XY plane as a whole.

Layer	Wavelength[m]	width[m]	length[m]	thickness[m]
ground	9.9E-2	8E-2	8E-2	3.5E-5
dielectric	9.9E-2	8E-2	8E-2	1.5E-3
patch	9.9E-2	3.13E-2	2.4E-2	3.5E-5

Table 3.2: Patch antenna parameter

With the above antenna structure, the scattering parameter S11 of the patch antenna performs well around the 3GHz frequency. For the consistency of the experimental results, the electric field data were collected on a spherical surface with a same radius of 0.2 [m] from the origin of the coordinates, although the three antennas have somewhat different structure sizes.

Chapter 4

Near field reconstruction result

In this section, the main focus is on the accuracy of the reconstructed fields in the near field for three different inverse source methods.In order to accurately measure the performance of the three inverse source methods, not only was the electric field reconstructed on the measurement sphere, but two spheres were selected as references, one inside and one outside it. The spherical radii are [0.18 0.19 0.21 0.22] m, respectively. Based on such experimental data, it is not only possible to analyze the reconstructed fields below the same sphere only in near-field conditions but also to compare the performance of the three inverse source methods on the inner and outer sides of the measurement surface.

From Fig 4.2 to Fig 4.11 are the reconstruction results of dipole antenna, while from Fig 4.12 to Fig 4.21 are the reconstruction results of dipole array antenna, and from Fig 4.22 to Fig 4.31 are the reconstruction results of patch antenna.Comparing the reconstructed results of each antenna in a particular sphere individually, it can be seen that the electric field error is usually less than 0 dB [v/m] compared to the measured and reconstructed electric field at most points where the mode of the electric field strength is greater than 30 dB [v/m]. In terms of the accuracy of reconstructed electric field, all three inverse source methods perform satisfactorily to some extent.

In order to visualize the reconstruction for different inverse source methods and different antennas, a line graph of the reconstruction field norm error for different antennas as the reconstruction spherical radius changes is shown in Fig 4.1, the reconstructed electric fields of the three different inverse source methods have an error of less than 3% compared to the reference electric field of the CST export. No matter the structure of the antenna is changed, it does not affect the accuracy of the reconstructed electric field too much. If accuracy of reconstruction field is the most important indicator to consider, *fitting* and *loveside* methods have a high application priority. From these two methods with higher accuracy, it can be seen that the inverse source method performs better in reconstructing the electric field closer to the measurement sphere, which is in accordance with the expectation that the error should show an increasing trend during the radiation of the electric field.

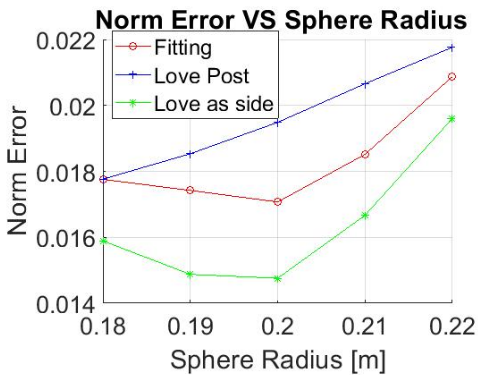

(a)

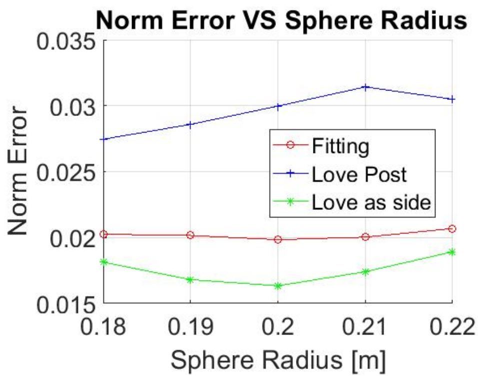

(b)

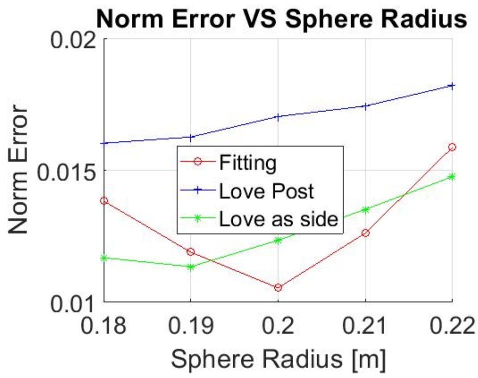

(c)

Figure 4.1: Norm error of (a)single dipole antenna (b)dipole array antenna (c)patch antenna

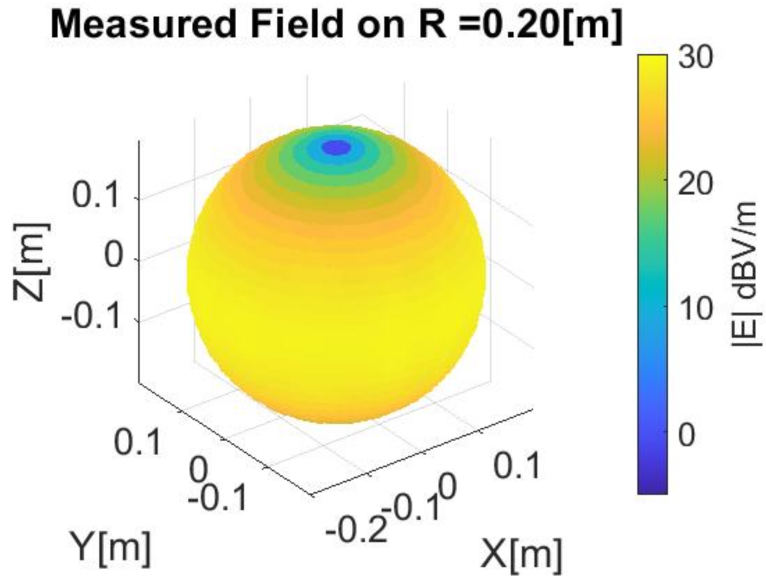

Figure 4.2: Dipole antenna measurement electrical field on the radius=0.2[m] spherical surface

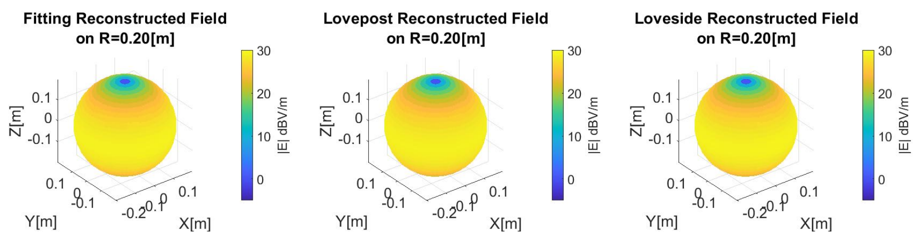

(a)

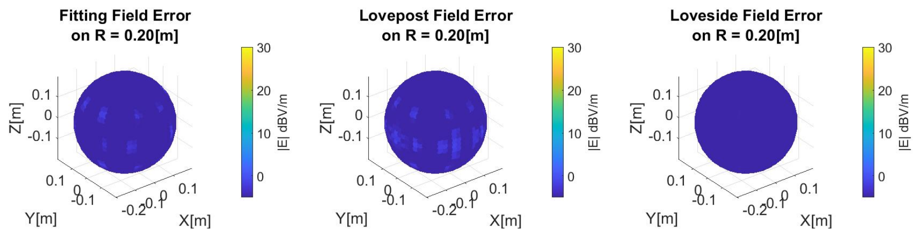

(b)

Figure 4.3: Dipole antenna three kinds of operators reconstructed electrical field on the radius=0.2[m] spherical surface(a)Reconstructed field (b) Field error refers to measurement electrical field

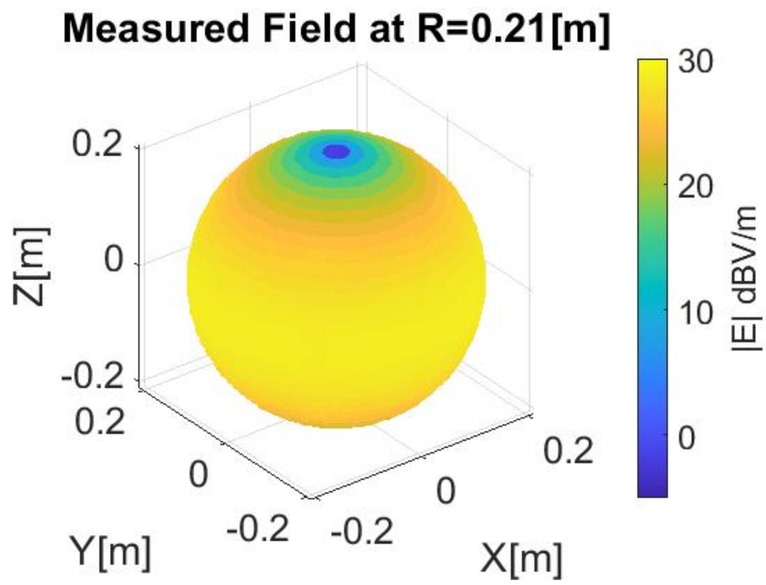

Figure 4.4: Dipole antenna measurement electrical field on the radius=0.21[m] spherical surface

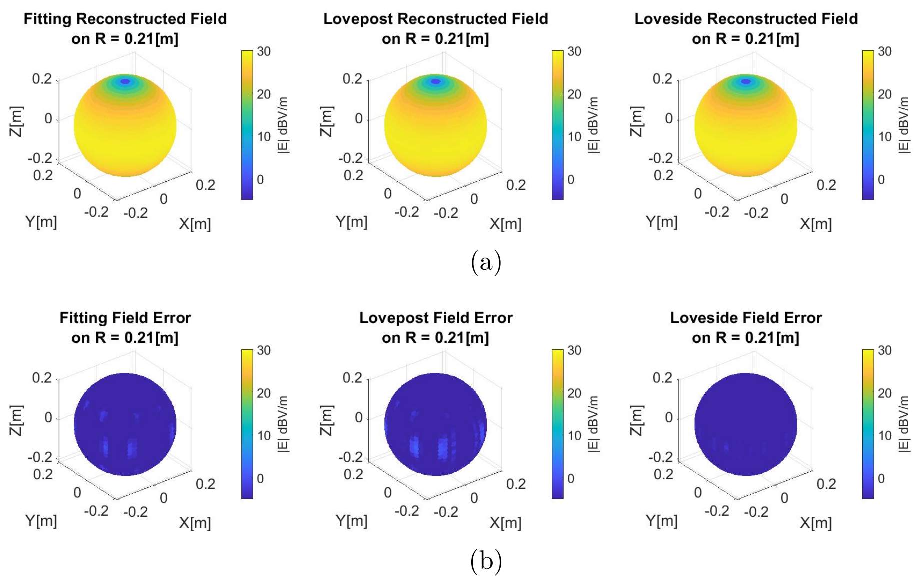

Figure 4.5: Dipole antenna three kinds of operators reconstructed electrical field on the radius=0.21[m] spherical surface(a)Reconstructed field (b) Field error refers to measurement electrical field

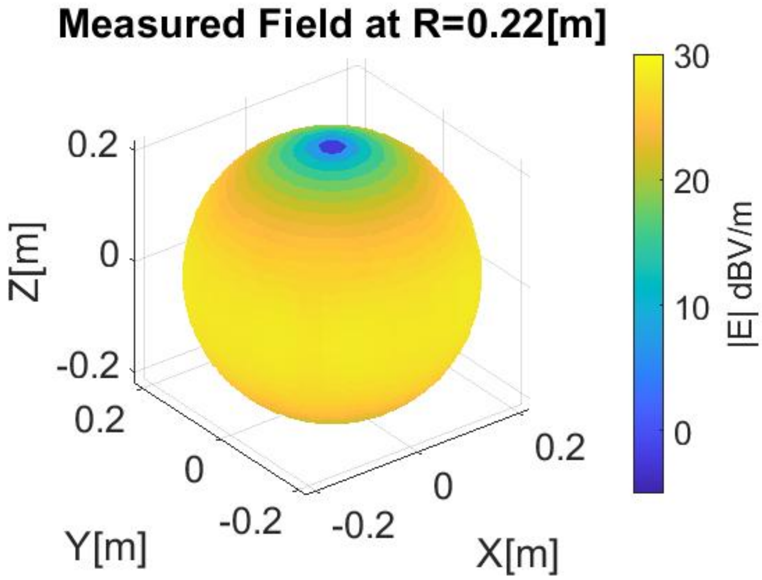

Figure 4.6: Dipole antenna measurement electrical field on the radius=0.22[m] spherical surface

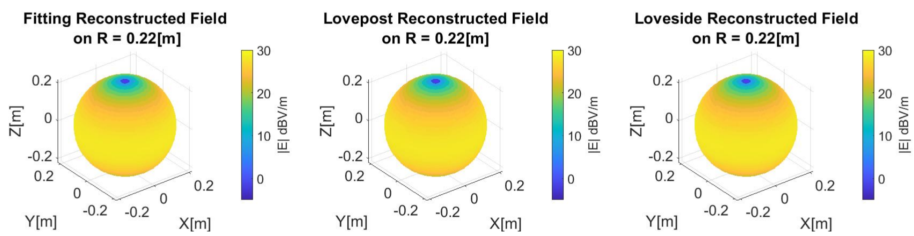

(a)

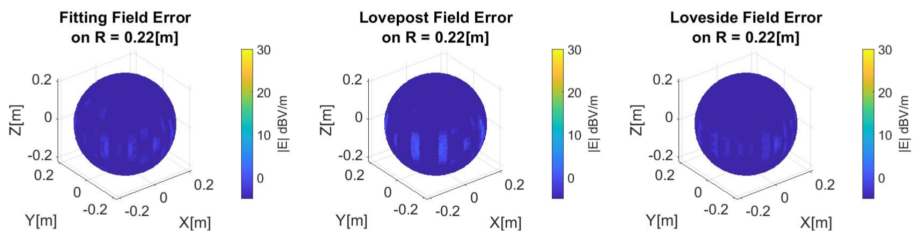

(b)

Figure 4.7: Dipole antenna three kinds of operators reconstructed electrical field on the radius=0.22[m] spherical surface(a)Reconstructed field (b) Field error refers to measurement electrical field

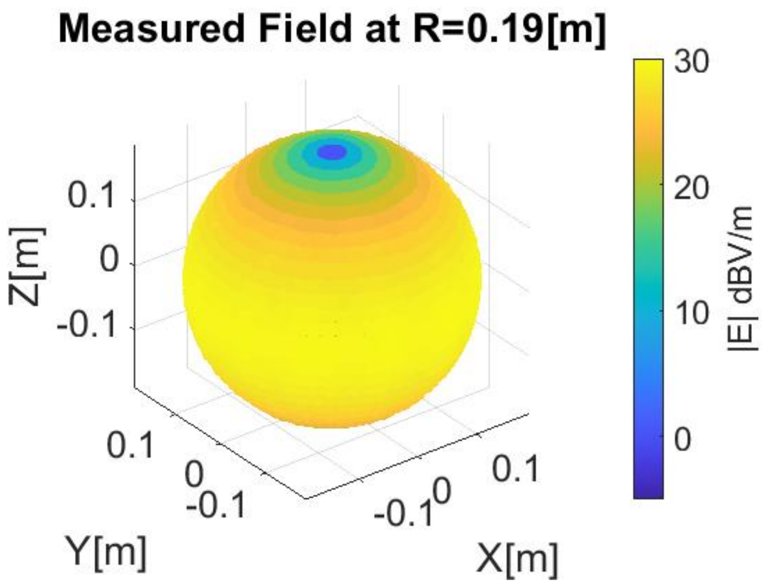

Figure 4.8: Dipole antenna measurement electrical field on the radius=0.21[m] spherical surface

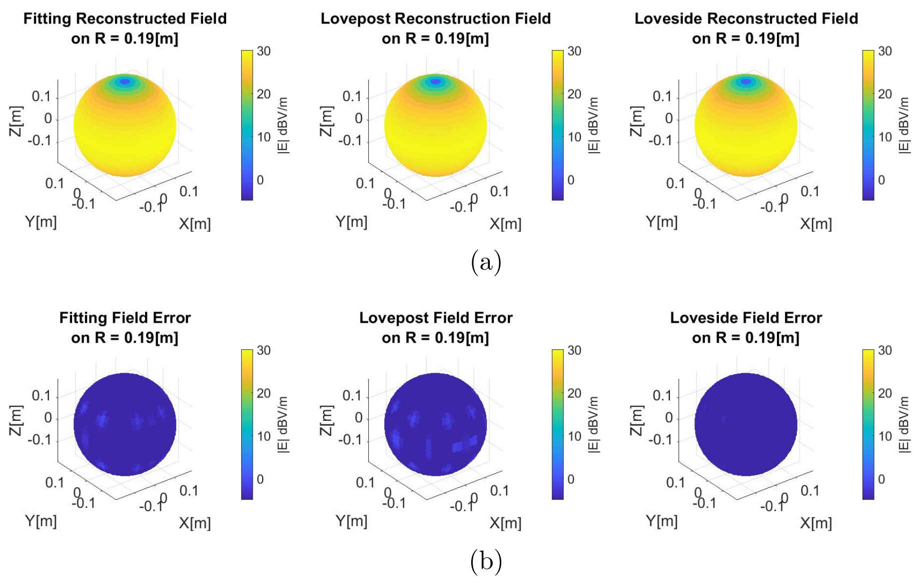

Figure 4.9: Dipole antenna three kinds of operators reconstructed electrical field on the radius=0.19[m] spherical surface(a)Reconstructed field (b) Field error refers to measurement electrical field

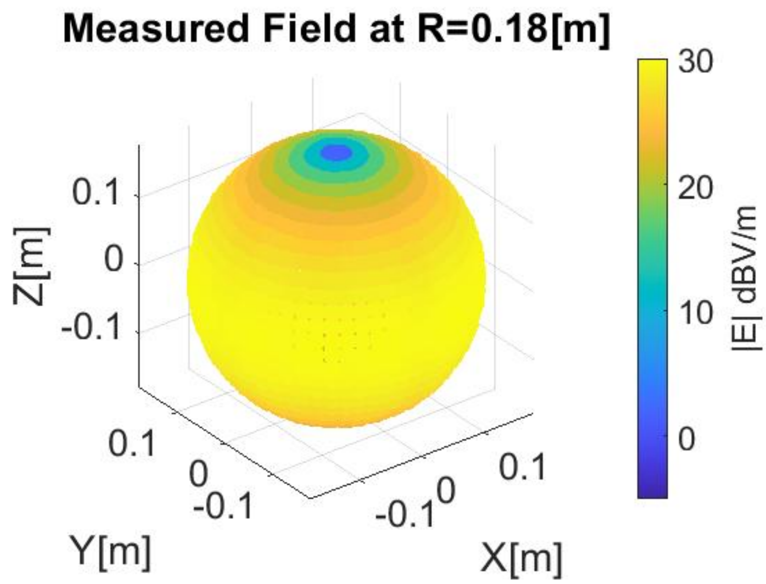

Figure 4.10: Dipole antenna measurement electrical field on the radius=0.18[m] spherical surface

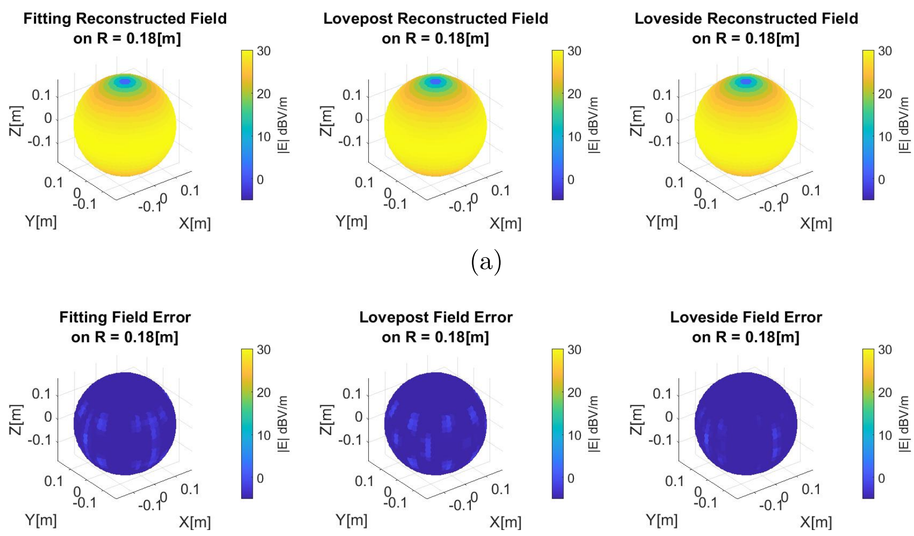

Figure 4.11: Dipole antenna three kinds of operators reconstructed electrical field on the radius=0.18[m] spherical surface(a)Reconstructed field (b) Field error refers to measurement electrical field

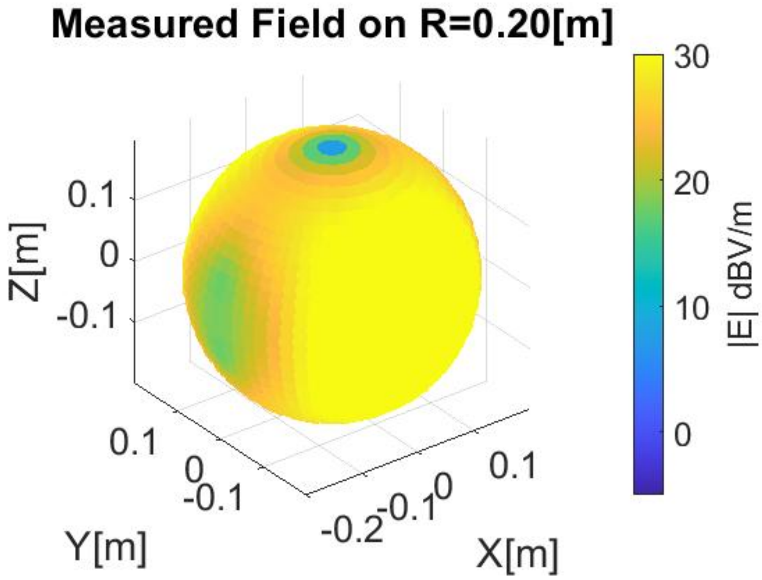

Figure 4.12: Dipole array antenna measurement electrical field on the radius=0.2[m] spherical surface

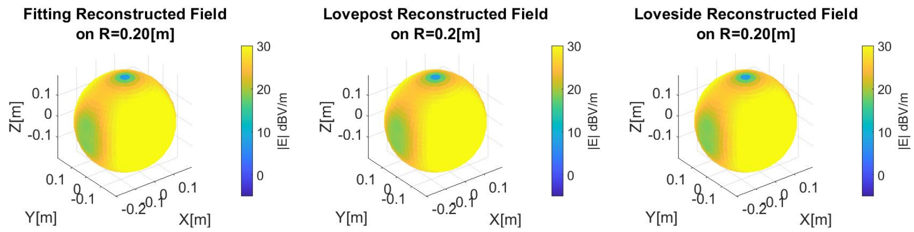

(a)

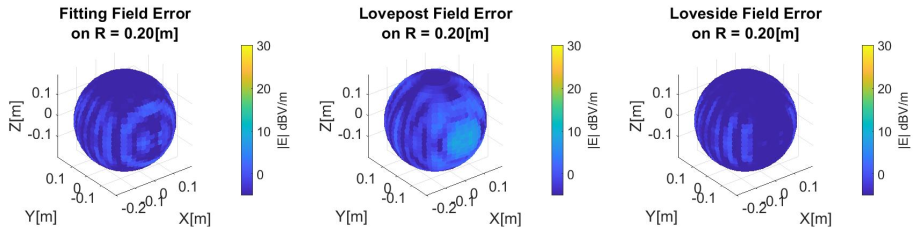

(b)

Figure 4.13: Dipole array antenna three kinds of operators reconstructed electrical field on the radius=0.2[m] spherical surface(a)Reconstructed field (b) Field error refers to measurement electrical field

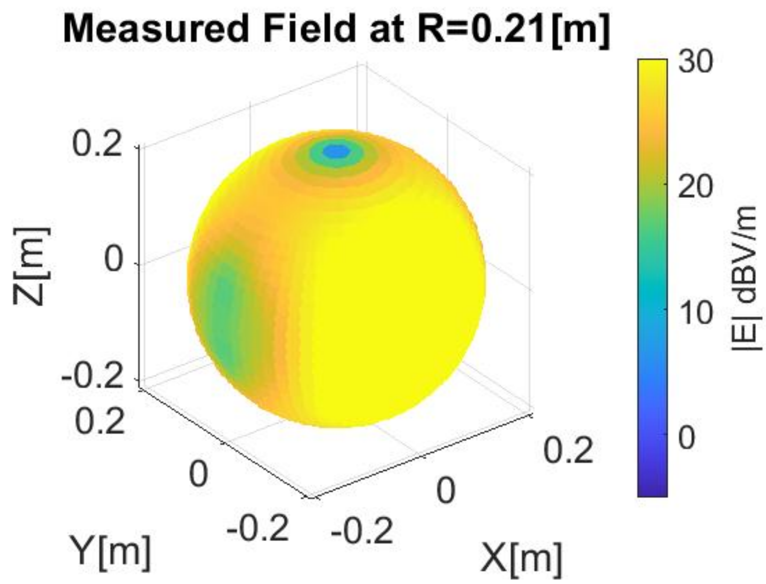

Figure 4.14: Dipole array antenna measurement electrical field on the radius=0.21[m] spherical surface

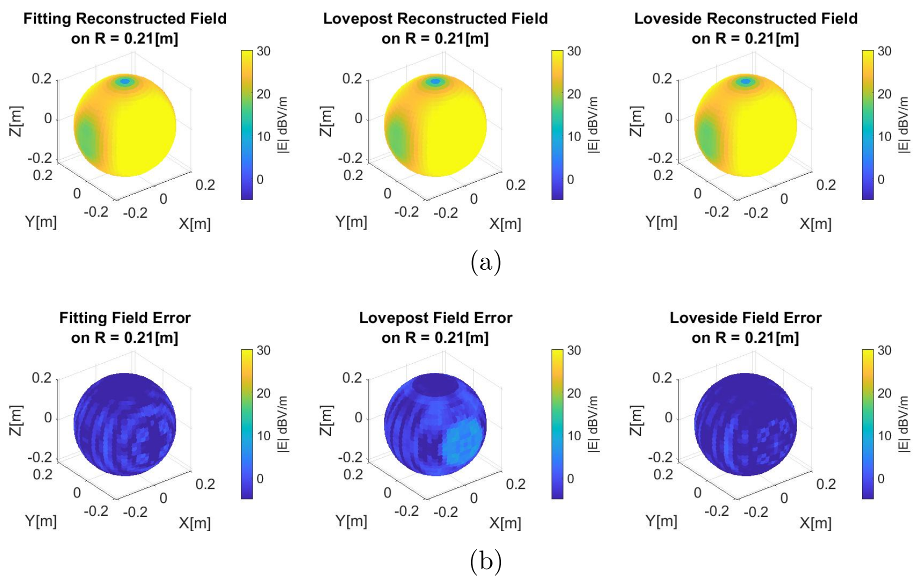

Figure 4.15: Dipole array antenna three kinds of operators reconstructed electrical field on the radius=0.21[m] spherical surface(a)Reconstructed field (b) Field error refers to measurement electrical field

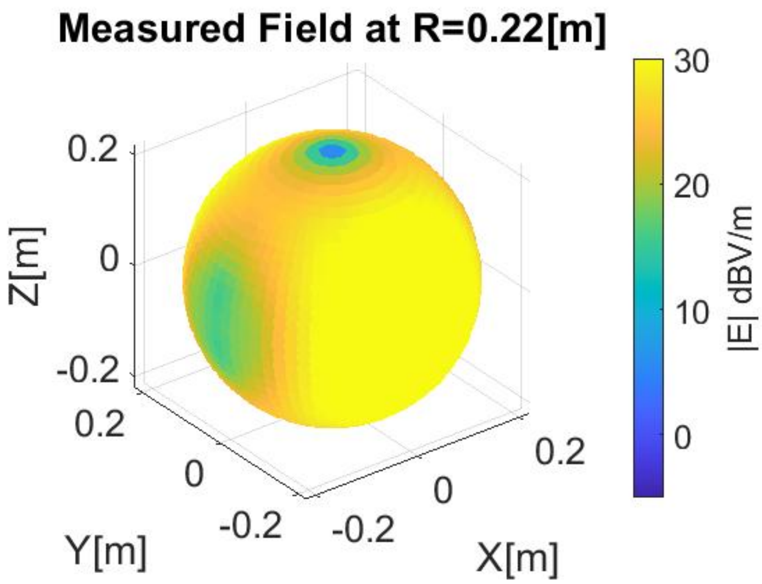

Figure 4.16: Dipole array antenna measurement electrical field on the radius=0.22[m] spherical surface

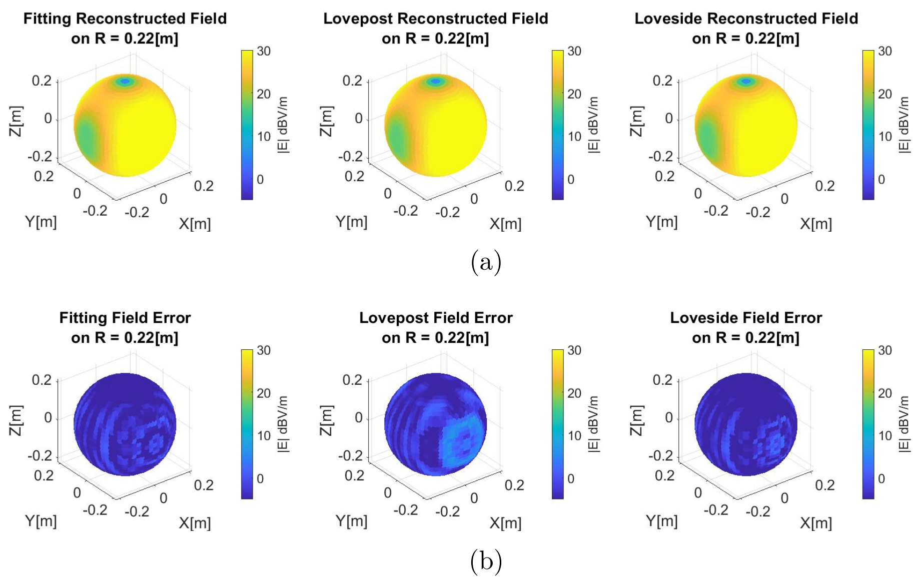

Figure 4.17: Dipole array antenna three kinds of operators reconstructed electrical field on the radius=0.22[m] spherical surface(a)Reconstructed field (b) Field error refers to measurement electrical field

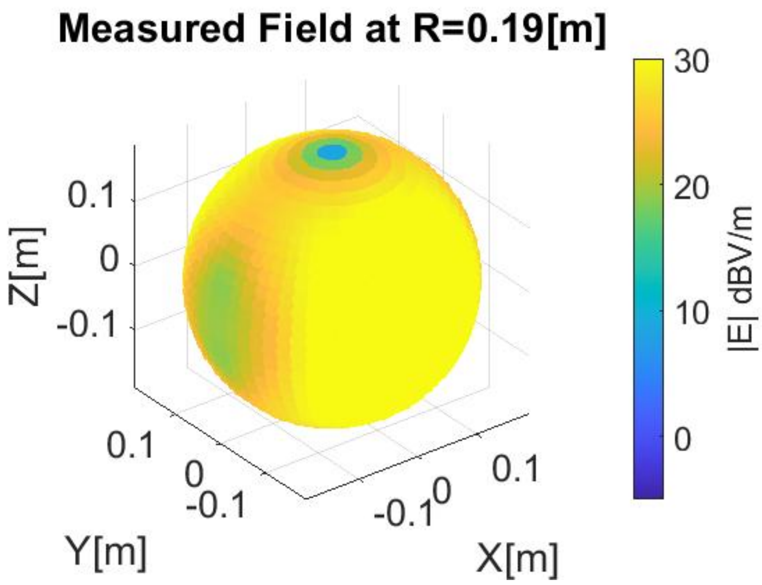

Figure 4.18: Dipole array antenna measurement electrical field on the radius=0.21[m] spherical surface

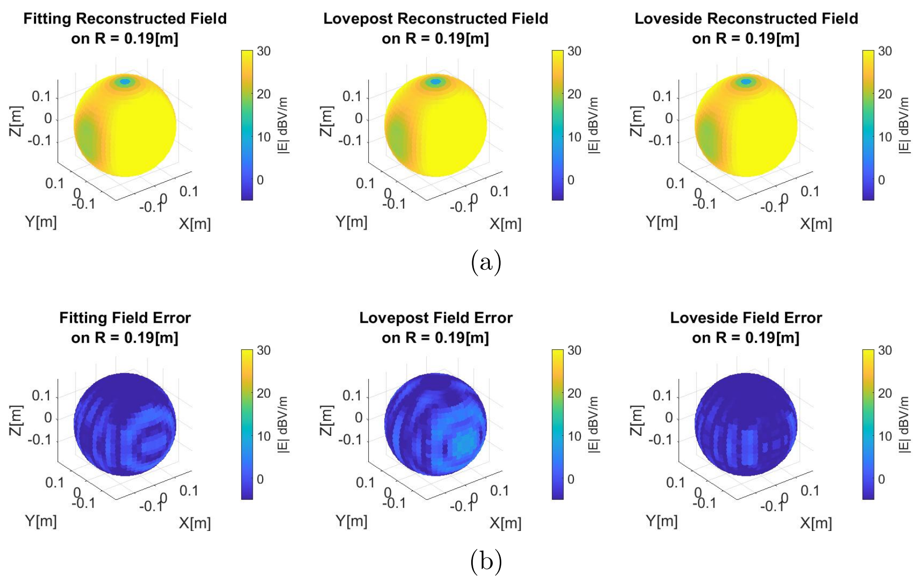

Figure 4.19: Dipole array antenna three kinds of operators reconstructed electrical field on the radius=0.19[m] spherical surface(a)Reconstructed field (b) Field error refers to measurement electrical field

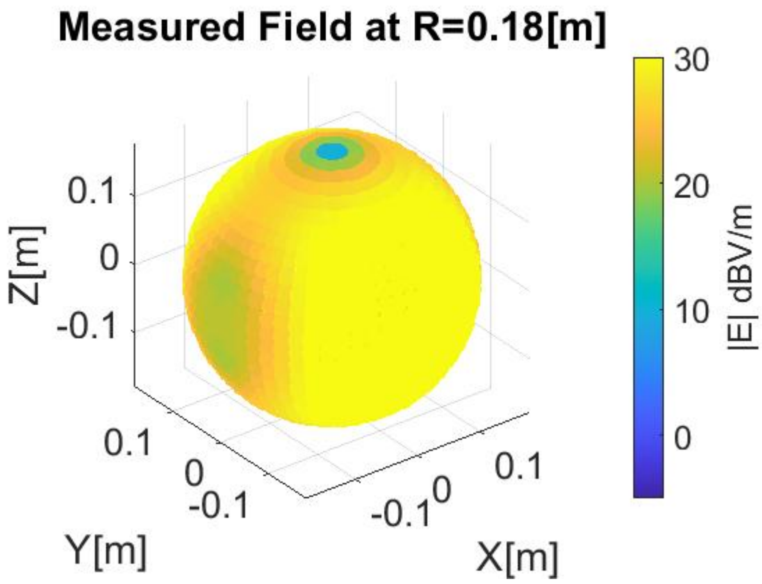

Figure 4.20: Dipole array antenna measurement electrical field on the radius=0.18[m] spherical surface

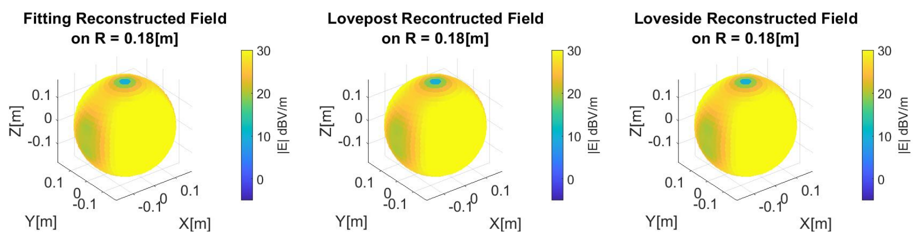

(a)

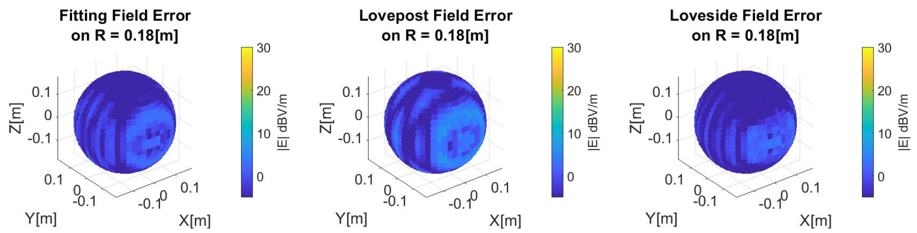

(b)

Figure 4.21: Dipole array antenna three kinds of operators reconstructed electrical field on the radius=0.18[m] spherical surface(a)Reconstructed field (b) Field error refers to measurement electrical field

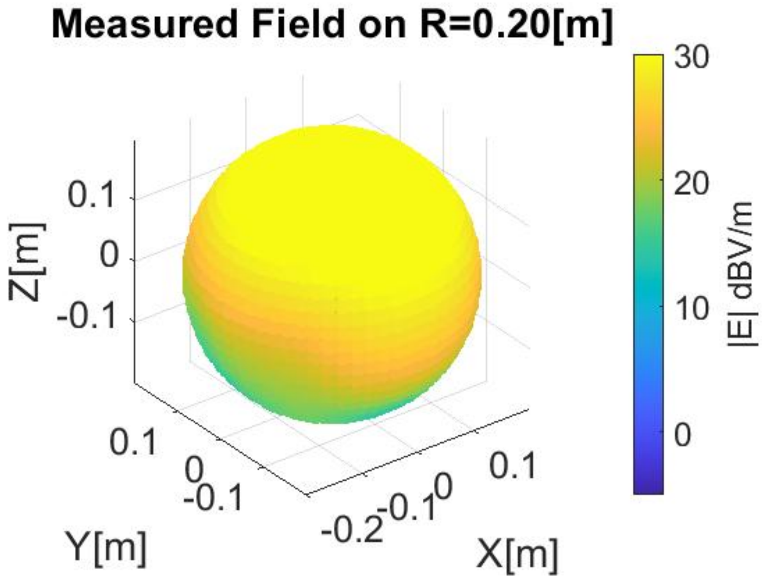

Figure 4.22: Patch antenna measurement electrical field on the radius=0.2[m] spherical surface

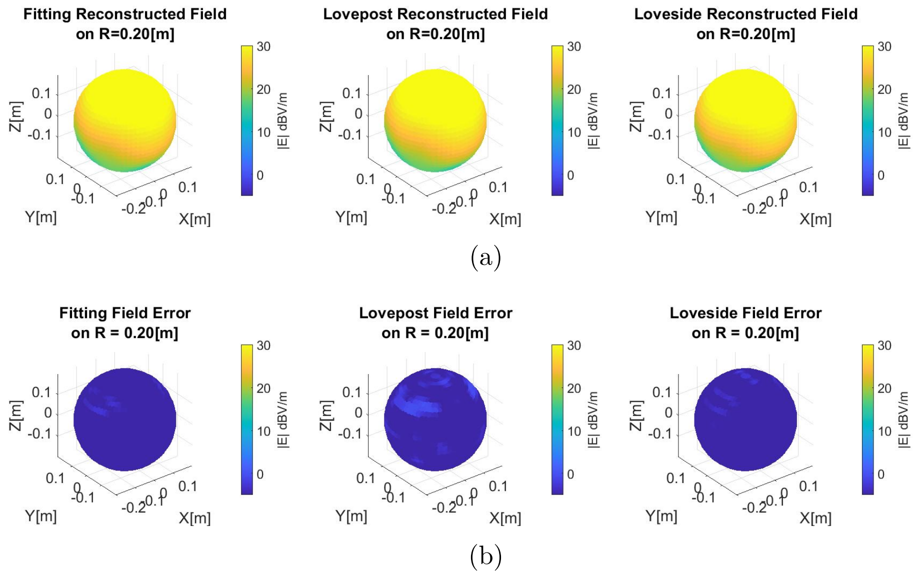

Figure 4.23: Patch antenna three kinds of operators reconstructed electrical field on the radius=0.2[m] spherical surface(a)Reconstructed field (b) Field error refers to measurement electrical field

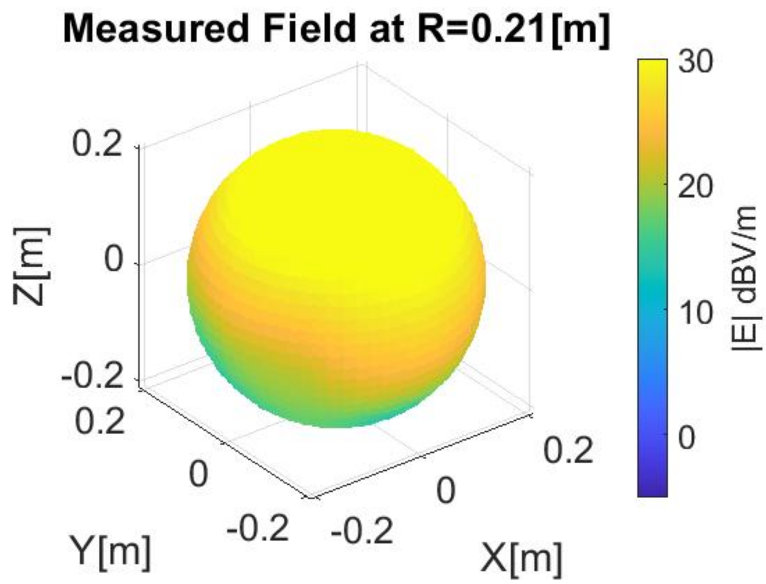

Figure 4.24: Patch antenna measurement electrical field on the radius=0.21[m] spherical surface

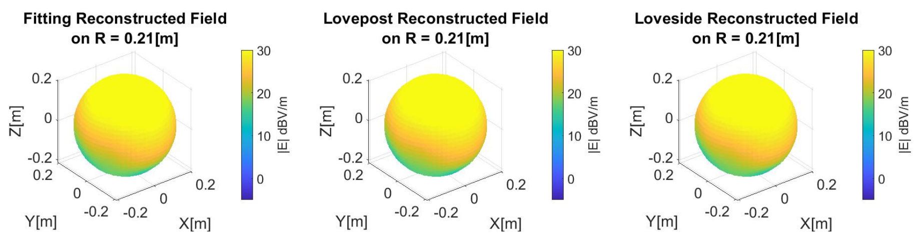

(a)

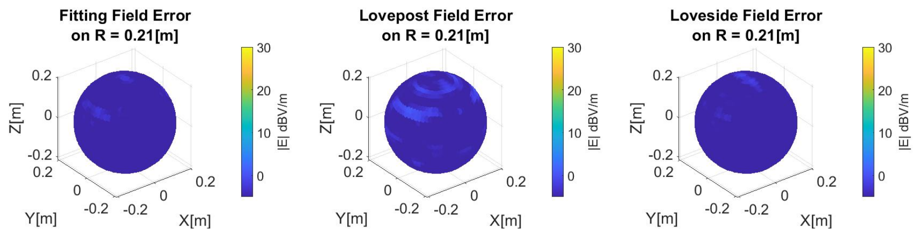

(b)

Figure 4.25: Patch antenna three kinds of operators reconstructed electrical field on the radius=0.21[m] spherical surface(a)Reconstructed field (b) Field error refers to measurement electrical field

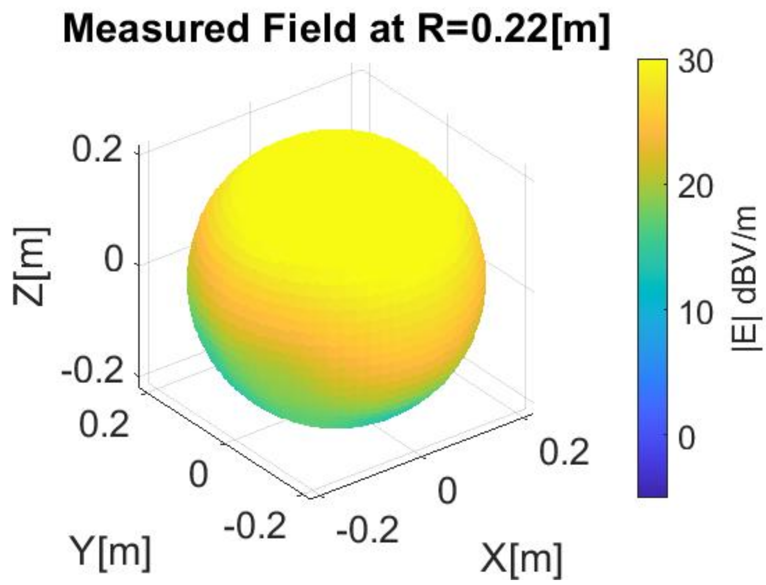

Figure 4.26: Patch antenna measurement electrical field on the radius=0.22[m] spherical surface

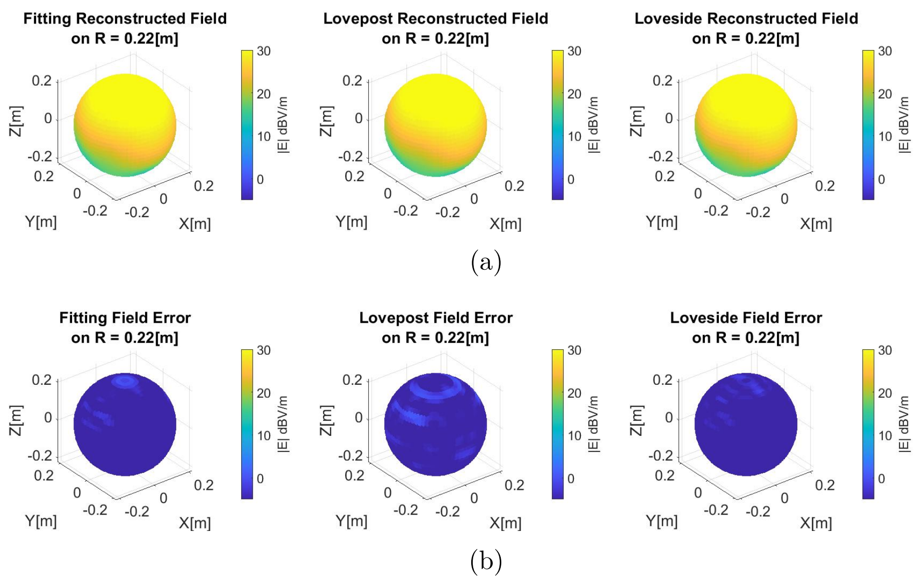

Figure 4.27: Patch antenna three kinds of operators reconstructed electrical field on the radius=0.22[m] spherical surface(a)Reconstructed field (b) Field error refers to measurement electrical field

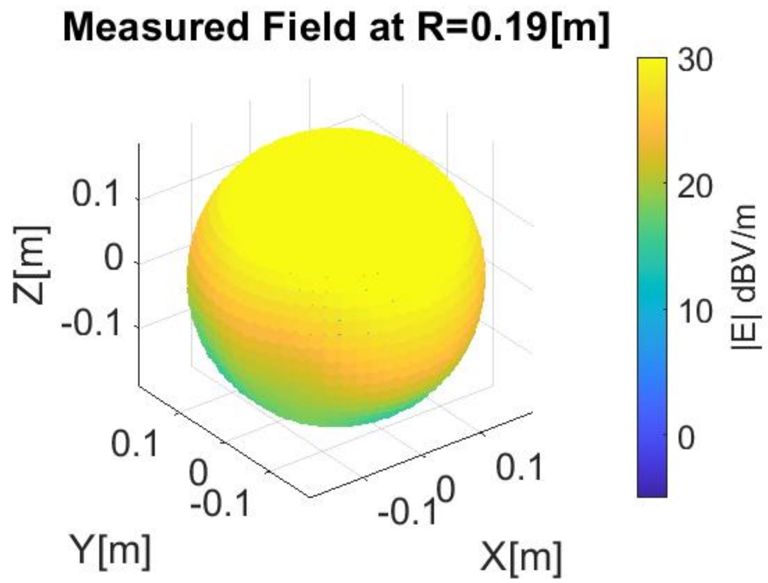

Figure 4.28: Patch antenna measurement electrical field on the radius=0.21[m] spherical surface

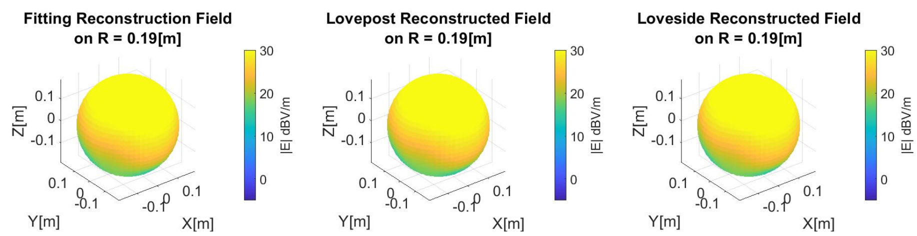

(a)

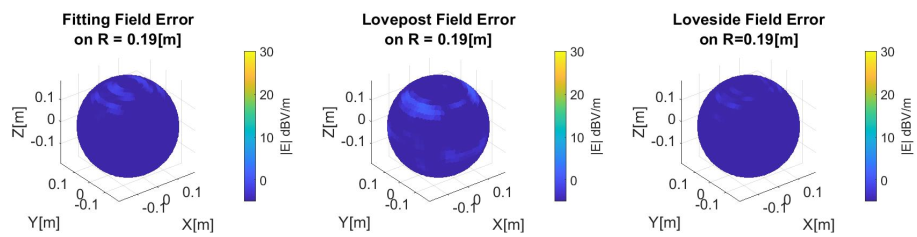

(b)

Figure 4.29: Patch antenna three kinds of operators reconstructed electrical field on the radius=0.19[m] spherical surface(a)Reconstructed field (b) Field error refers to measurement electrical field

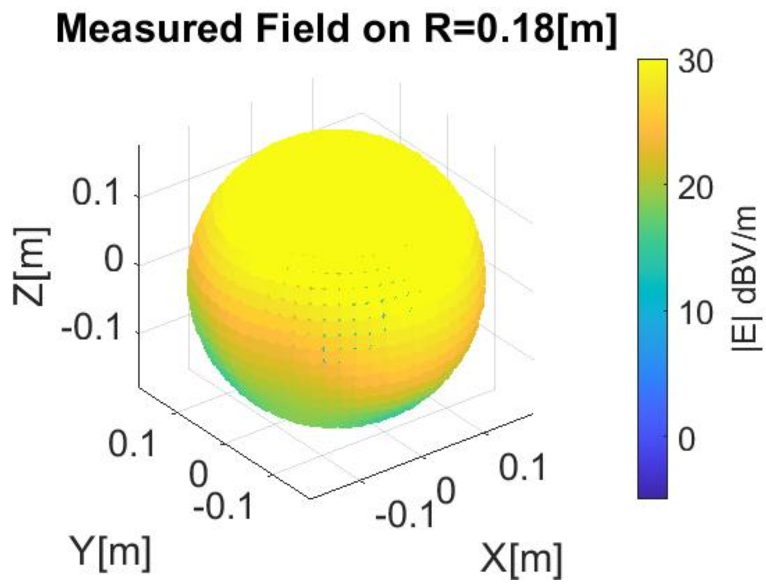

Figure 4.30: Patch antenna measurement electrical field on the radius=0.18[m] spherical surface

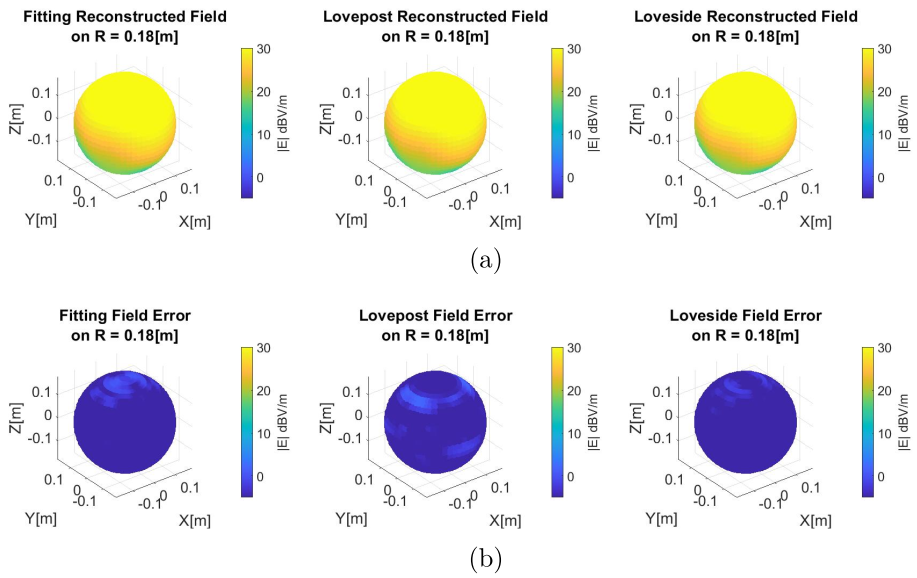

Figure 4.31: Patch antenna three kinds of operators reconstructed electrical field on the radius=0.18[m] spherical surface(a)Reconstructed field (b) Field error refers to measurement electrical field

Chapter 5

Far field reconstruction result

After discussing playing with near-field reconstruction, this chapter turn attention to far-field reconstruction. As the near-field reconstructed electric field, the far field corresponding to the three antennas will be reconstructed based on three different inverse source methods.In order to have a better reference for the far field, the far fields of three different antennas are plotted in matlab in 3D. It is important to note that all far-fields are discussions of the radiation pattern, and not to reconstruct the field on a particular surface.

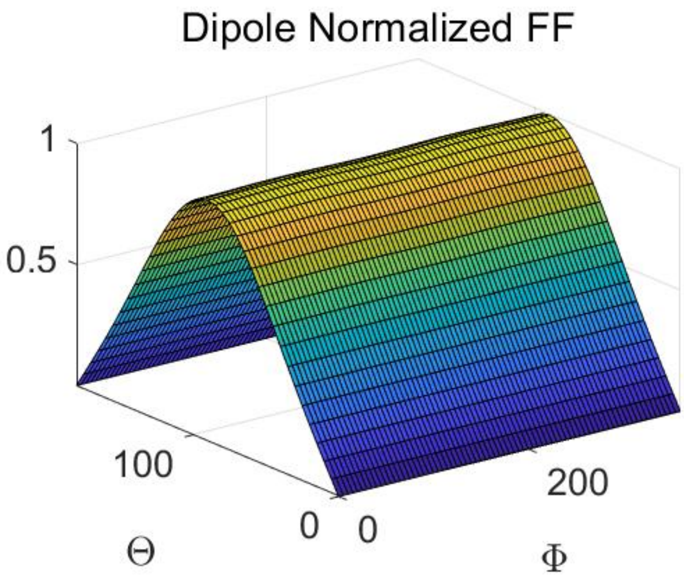

Figure 5.1: Dipole antenna far-field electrical field

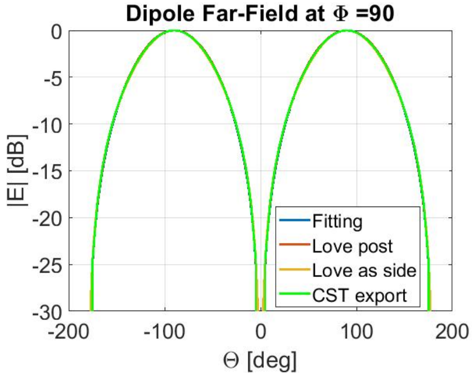

(a)

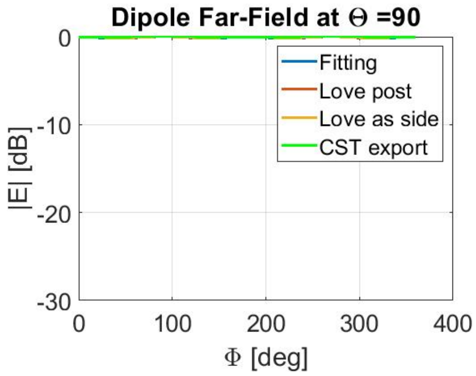

(b)

Figure 5.2: Dipole antenna far-field electrical field cut (a)$\phi = 90$ degree (b) $\theta = 90$ degree

From Fig 5.1 to Fig 5.6 below, the reconstructed far fields of the three inverse source methods are almost identical to the simulation results of the CST studio suite. It also fits the far-field image of 3D, which argues the accuracy from another perspective. The far-field reconstruction using equivalent surface currents and surface magnetic currents can be considered as a flawless restoration of the real far-field distribution. It is also observed that the simulated export data tends to be smoother in the case of rapid decay of the electric field intensity. By increasing the sampling density and improving the accuracy of the algorithm, there will be a better fit to the curve but also a significant uplift in simulation and computing time.

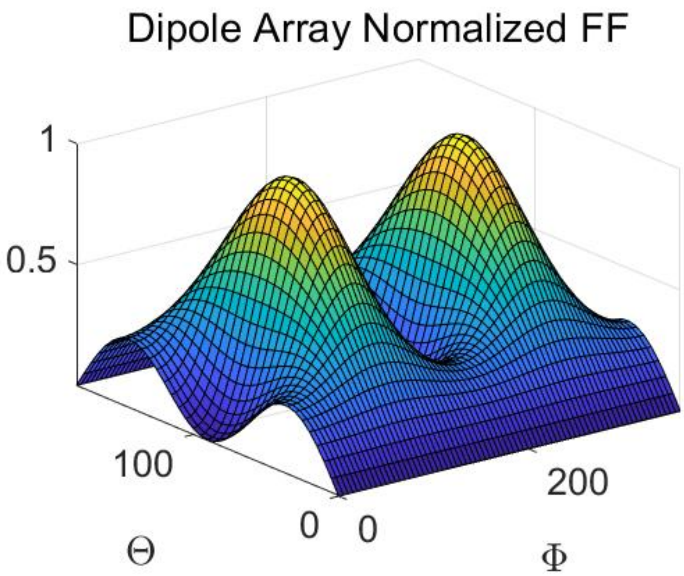

Figure 5.3: Dipole array antenna far-field electrical field

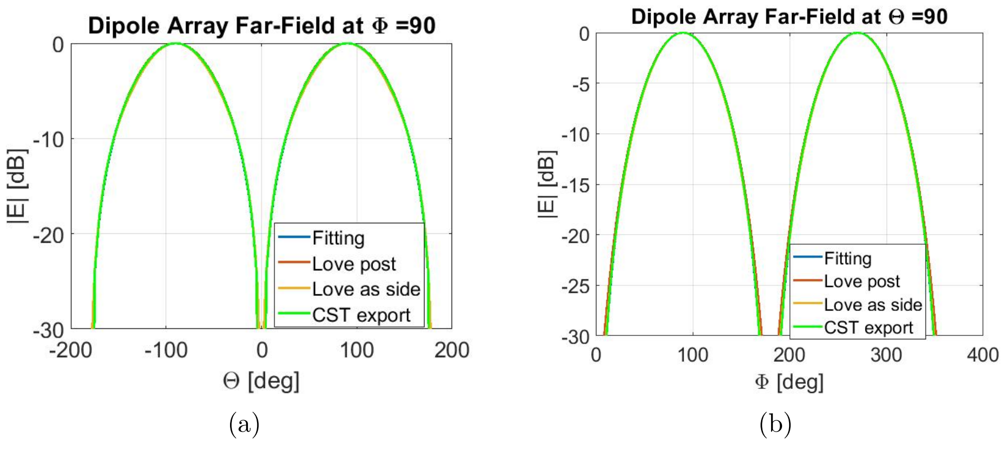

Figure 5.4: Dipole array antenna far-field electrical field cut (a)$\phi = 90$ degree (b) $\theta = 90$ degree

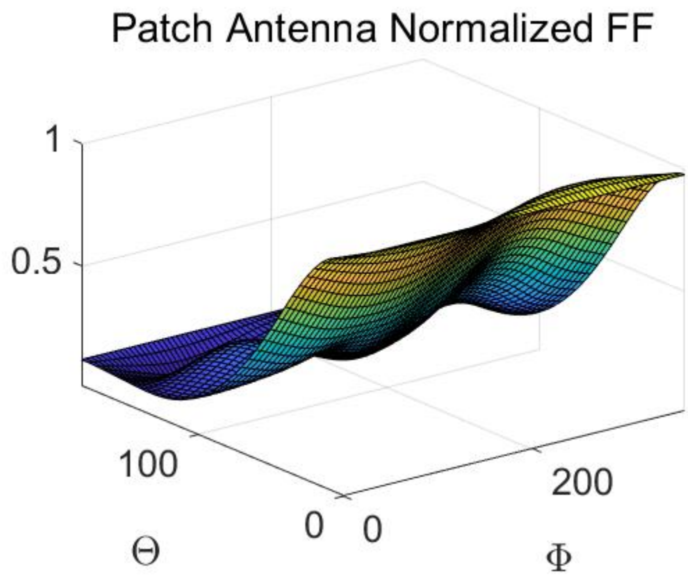

Figure 5.5: Patch antenna far-field electrical field

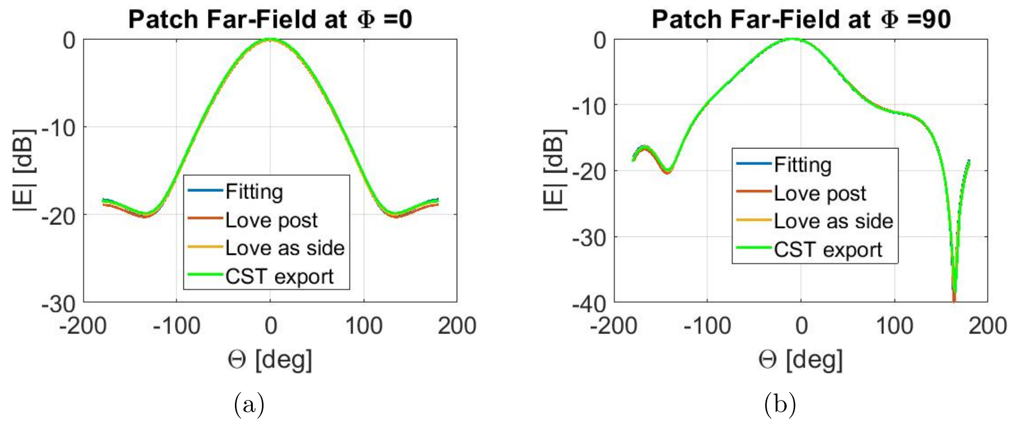

Figure 5.6: Patch antenna far-field electrical field cut (a)$\phi = 0$ degree (b) $\phi = 90$ degree

Chapter 6

Conclusion

After the present analysis, it is evident that the three inverse source methods have an adequate accuracy and generality in reconstructing the electric field. In circumstances where high accuracy is essential for near-field reconstruction, it is more sensible to choose the *loveside* operator. However, it must be stated that the *lovepost* operator expends less computational resources whether in terms of time or memory usage than the *loveside* operator. Although the gap is not significant in the current experiments, it is apparent that under more complex antenna models or more spatially varied electric field conditions, the measurement data set will become much more massive for accuracy. Moreover, the complexity of the operational matrix will grow in square steps. The specific trade-off will be further studied in the future. In the case of considering the distance between the reconstructed electric field and the measured electric field, the error is proportionally smaller for closer reconstructed surfaces. The explanation for this is that either operator first coincides with the measured electric field to produce the equivalent current, and the accuracy of the calculation needs to be adjusted to the reconstruction surface distance. All three inverse source methods are quite good when considering the performance in far-field situations. The far field will be a frequent case compared to the size of part of the antenna itself. The inverse source method will be more applicable to the far-field problem, and subsequent studies will be extended to real antennas to better examine it.

Bibliography

[1] P. Petre and T.K. Sarkar. «Planar near-field to far-field transformation using an equivalent magnetic current approach». In: *IEEE Transactions on Antennas and Propagation* 40.11 (1992), pp. 1348–1356. DOI: 10.1109/8.202712 (cit. on p. 1).

[2] A. Taaghol and T.K. Sarkar. «Near-field to near/far-field transformation for arbitrary near-field geometry, utilizing an equivalent magnetic current». In: *IEEE Transactions on Electromagnetic Compatibility* 38.3 (1996), pp. 536–542. DOI: 10.1109/15.536088 (cit. on p. 1).

[3] T.K. Sarkar and A. Taaghol. «Near-field to near/far-field transformation for arbitrary near-field geometry utilizing an equivalent electric current and MoM». In: *IEEE Transactions on Antennas and Propagation* 47.3 (1999), pp. 566–573. DOI: 10.1109/8.768793 (cit. on p. 1).

[4] B. Nadeau and J.-J. Laurin. «Extrapolations using vectorial planar near-field measurements for EMC applications». In: *1998 IEEE EMC Symposium. International Symposium on Electromagnetic Compatibility. Symposium Record (Cat. No.98CH36253).* Vol. 2. 1998, 924–928 vol.2. DOI: 10.1109/ISEMC.1998.750331 (cit. on p. 1).

[5] J.-J. Laurin, J.-F. Zurcher, and F.E. Gardiol. «Near-field diagnostics of small printed antennas using the equivalent magnetic current approach». In: *IEEE Transactions on Antennas and Propagation* 49.5 (2001), pp. 814–828. DOI: 10.1109/8.929636 (cit. on p. 1).

[6] F. Las-Heras, M.R. Pino, S. Loredo, Y. Alvarez, and T.K. Sarkar. «Evaluating near-field radiation patterns of commercial antennas». In: *IEEE Transactions on Antennas and Propagation* 54.8 (2006), pp. 2198–2207. DOI: 10.1109/TAP.2006.879190 (cit. on p. 1).

[7] Javier Leonardo, Araque Quijano, and Giuseppe Vecchi. «Removal of unwanted structural interactions from antenna measurements». In: *2009 IEEE Antennas and Propagation Society International Symposium.* 2009, pp. 1–4. DOI: 10.1109/APS.2009.5172309 (cit. on p. 1).

[8] Javier Leonardo Araque Quijano and Giuseppe Vecchi. «Improved-Accuracy Source Reconstruction on Arbitrary 3-D Surfaces». In: *IEEE Antennas and Wireless Propagation Letters* 8 (2009), pp. 1046–1049. DOI: `10.1109/LAWP.2009.2031988` (cit. on p. 1).